Journal of Energy Storage 79 (2024) 110233

Contents lists available at ScienceDirect

Journal of Energy Storage

journal homepage: www.elsevier.com/locate/est

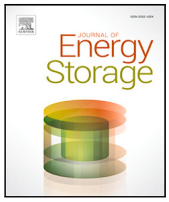

Research papers

Battery configuration dependence to power line communication using high-order quadrature amplitude modulation☆

Mahyar J. Koshkouei *, Erik Kampert[1], Andrew D. Moore, Matthew D. Higgins

WMG, University of Warwick, CV4 7AL, Coventry, United Kingdom

ARTICLE INFO

Keywords:
Power line communication
Quadrature amplitude modulation
Smart batteries
Lithium-ion
Intelligent vehicles

ABSTRACT

Power line communication (PLC) within future smart batteries facilitates the communication of high fidelity sensor data between smart cells and external systems, with application areas including intelligent vehicles and smart grids. This interconnected PLC system of smart cells will enhance cell utilisation and safety through cell-to-cell coordination at a system level, leveraging the existing bus bar within the battery and eliminating the need for additional wire harnesses. This paper studies the performance of a PLC system operating at carrier frequencies of 10 MHz to 6 GHz within four distinct configurations of lithium-ion batteries. This assessment focuses on changes in scattering parameters and data transmission error ratios. Furthermore, quadrature amplitude modulation (QAM) orders of up to 1024 are investigated for their viability within such environments. The results indicate that the addition of cells in parallel increases error ratios with high-order QAM, and that this effect varies substantially with carrier frequency. Using QAM increases data throughput, allowing for data transfers within large-scale battery systems without PLC bus bandwidth saturation. A prospective centre frequency of 3650 MHz allows for a wide bandwidth of 300 MHz and 1024-QAM with little signal attenuation and data error. At this frequency, the need for signal repeaters and higher signal output power is reduced. These results are used to determine the most suitable arrangement of cells within a smart battery with consideration of the PLC performance. The preliminary performance of a large-scale battery system with PLC in-situ could be derived from the findings in this research based upon the four battery configurations tested.

1. Introduction

The use of renewable energy has received greater attention due to the climate emergency. To reduce the output of carbon emissions in transportation, the battery electric vehicle (BEV) can be charged with renewable energy. However, the BEV is currently unable to outperform existing internal combustion engine vehicles by global market share — due to its comparatively long charging times, reduced travel distances on a single charge, and perceived high purchase and running costs [1].

To mitigate these disadvantages in BEVs, the established literature demonstrates improvements to energy storage systems, such as fast charging techniques, improved battery safety, and efficiency [2]. The BEV energy storage system typically utilises lithium-ion (Li-ion) cells due to their high energy and power density, lack of memory effect, and high efficiency, when compared to other battery chemistries such as nickel-metal hydride and lead–acid [3]. However, there are challenges facing the use of Li-ion cells, notably their safety when over-charging, over-discharging, or exceeding fast charging limits defined by the manufacturer. In these circumstances, the Li-ion cell may be permanently damaged, but may also enter a thermal runaway state which can cause fire and even explosion [4]. This problem can be resolved by using a battery management system (BMS), which generally consists of important features such as cell balancing, state of charge (SoC) and state of health (SoH) monitoring [5]. However, these safety features limit the potential performance of the Li-ion cells as the BMS makes assumptions, or based on limited monitoring, related to their characteristics, such as internal temperatures. This constraint exists because typical Li-ion cells do not currently have a temperature sensor embedded within to allow for the BMS to obtain internal temperature data. Therefore, the surface temperature must be used as a safety measure to protect against cell

☆ *Abbreviations*: ASK, amplitude shift keying; BER, bit error rate; BEV, battery electric vehicle; BMS, battery management system; CAN, controller area network; EMI, electromagnetic interference; EVM, error vector magnitude; FSK, frequency shift keying; Li-ion, lithium-ion; OOK, on-off keying; PLC, power line communication; QAM, quadrature amplitude modulation; SER, symbol error rate; SoC, state of charge; SoH, state of health; VNA, vector network analyser; VST, vector signal transceiver.

* Corresponding author.
E-mail address: mahyar.j.koshkouei@warwick.ac.uk (M.J. Koshkouei).
[1] Current address: Institute of Fundamentals of Electrical Engineering, Helmut Schmidt University, 22043, Hamburg, Germany

https://doi.org/10.1016/j.est.2023.110233
Received 1 February 2023; Received in revised form 15 December 2023; Accepted 19 December 2023
Available online 9 January 2024

Table 1
Comparison of various smart battery communication methods. A summary of literature on PLC systems for Li-ion cells is shown in Table 1.

Smart battery network topology	Wire harness required	Complexity & cost	Comments
None	Wire required to connect each sensor embedded within each cell to an external BMS.	High	The number of wires required for a battery of many smart cells to be connected in this way adds significant weight, cost, and complexity to the battery system. In addition, the robustness of the assembly is compromised especially when subject to high vibration environments.
Two-Wire [7]	Two wires required to be connected to each smart cell.	Medium	The two wires will add some weight and complexity to the system. Changes to the battery architecture are still required to accommodate the extra wire harness.
Wireless [8]	None.	Medium	The performance of the wireless network may be degraded due to multipath effects and shielding caused by other cells in the battery. The modifications to the smart cell required to integrate a wireless antenna increases the complexity and cost of this method. This technique requires further research for its suitability in batteries.
PLC	None.	Low	The bus-bar is used as the communication channel, so changes to the battery architecture and layout are not required. The use of PLC within the Li-ion battery is under investigation in this paper for its suitability in various battery configurations.

thermal runaway. However, the established literature has demonstrated that the internal temperature of the cell is much hotter than the surface temperature during fast charging and discharging [6].

In the following studies based on the topic of cell instrumentation, the sensors embedded within the cell are connected to an external data acquisition device, such as an analogue to digital converter (ADC), to record the temperature. Using electrically based sensors or optical monitoring, a battery pack of many instrumented cells would require a large and heavy wire and/or optical harness to accommodate the wired connections for each sensor embedded within each cell. Coupled with the BMS, the research community has been instrumenting cells using embedded sensors to improve real time analysis [9]. This includes analysis of the internal temperature of the cell during fast charging and discharging. An additional benefit being, for example, is that by combining a cell instrumentation technique with a constant-temperature constant-voltage charging scheme, charging times may be reduced by up to 20 % [10]. One such technique includes embedding fibre optics within the Li-ion cell to monitor internal cell temperature [11]. In this research, a Rayleigh back-scatter based optical fibre sensor was embedded within a 21700-model cylindrical Li-ion cell and it was determined that the internal temperature was 9.7 °C higher than the surface temperature during a 1 charge-rate discharge. This large difference in temperature means that whilst a BMS is taking into account the surface temperature of the Li-ion cell to enforce safety limits, the core may already be exceeding these safety limits by nearly 10 °C. Hence, the Li-ion cell may have actually been closer to a thermal runaway event than originally anticipated. Similar techniques include the use of thermocouples for core temperature sensing within a 21700-model cylindrical Li-ion cell [12] and within a pouch and 18650-model Li-ion cell [13]. These research studies have revealed significant temperature differences of up to 4 °C and 13 °C between the core and surface of the cells during cell discharge, respectively.

The capability for monitoring and analysis of data from embedded sensors in instrumented cells by the BMS is underpinned by the communication system [14]. Such a communication system normally requires a wire harness independent of the bus bar to use as a communication bus. This wire harness increases the weight of the battery pack, and hence reduces its power and energy density and also requires non-standard cell formats to be used with extra connections. A comparison of experimental communication methods for potential instrumented Li-ion cells is shown in Table 1. A two-wire communication bus has been presented in [7], whereby the communication bus was also able to power the embedded system on the cell rather than consume power from the cell itself. For large-scale batteries with many cells, using a wire harness to connect each instrumented cell to the BMS would increase the battery complexity and cost. Alternatively, a wireless communication method may be used as demonstrated within a test laboratory in [8]. However, further research is required to determine the performance of such wireless system within the complex structures of large-scale batteries, and to test this wireless system when integrated within a real Li-ion cell. Therefore, a communication system must be utilised that does not require any additional wire harness within the battery, and allows for instrumented cells within the battery pack to send sensor measurements to the BMS.

A communication system operating within a battery system of smart cells that are instrumented with temperature sensors would realise the transfer of the internal cell temperature measurement data from each of the smart cells to the BMS. The BMS will use this measurement data to determine the cells SoC, SoH, and other parameters to make appropriate safety and performance decisions. These decisions may include reducing the power output of the battery system in order to reduce the temperature of the Li-ion cells, or increasing the charging current if the cell core temperatures are under a safe threshold.

For a large-scale battery system of thousands of smart cells, the amount of data being transferred from each smart cell to the BMS will become significant. This complexity is exacerbated by the fact that the temperature of the Li-ion may increase rapidly depending on use. Hence, the response time of the BMS to receive critical temperature measurement data and enact safety critical features must be as short as possible. In addition, the data being transferred from the smart cells to the BMS may increase in the future as additional sensors, such as a local cell fuel gauge sensor, are integrated within the smart cell. Furthermore, a bi-directional system, enabling the BMS to communicate with each individual smart cell, will allow for the BMS to command specific smart cells to perform necessary appropriate actions, such as reconfiguring the battery by removing specific smart cells from the circuit using in-situ cell MOSFETs [15]. Such in-situ cell MOSFETs may also be used to heat up the cell to an optimum temperature in very cold climates [16].

Based on these facts, power line communication (PLC) is selected for potential use in this application. PLC is a communication technology that uses the existing power bus, such as the battery bus bar, for data transmission. Therefore, an additional wire harness is not required for a PLC system. For similar reasons, it is straightforward to install a PLC system and it can be used in power outlets common in homes, buildings, and other facilities. In these applications, a PLC channel suffers from interference caused by electrical appliances such as switching power supplies and motors. Similarly, a large-scale battery system within a

BEV will also suffer from the same properties that make the physical channel a harsh environment for PLC. Furthermore, the power line network may use varying conductor types, cross sections joints, and termination impedances which make the power line a challenging medium to operate in [17]. The impedance will also change as the load on the power line changes, due to consumer use for example. Impedance mismatch causes a multipath effect, whereby the signal propagates onto additional paths causing it to arrive at the receiver at different time intervals, which can cause a reduction or amplification in the signal amplitude or even nullification if the signals arrive 180 degrees out of phase. These effects can cause data corruption and/or loss. Various standards, such as HomePlug and IEEE 1901, exist to overcome the harsh conditions of the power line channel [18]. In these standards, orthogonal frequency-division multiplexing (OFDM) is used with equally spaced subcarriers to improve bandwidth efficiency and reduce the effects of multipath fading. OFDM is a technique that divides wideband into multiple narrowband subcarriers, each of which is modulated using a different carrier frequency that is mathematically orthogonal to the carrier frequencies of the other subcarriers [19]. The subcarriers may be modulated using phase shift keying, but the most recent PLC standards, such as HomePlug AV2 allow for the use of QAM up to a modulation order of 4096. By utilising OFDM with 3455 equally spaced subcarriers in the range of 1.8 MHz to 86.13 MHz and using 4096-QAM, amongst other technical advancements such as MIMO (multiple input multiple output), HomePlug AV2 is capable of reaching a maximum physical layer rate to 2024 Mbit/s [20,21]. QAM is a modulation scheme that utilises variations in both amplitude and phase of a carrier signal [22]. By manipulating the amplitude and phase of the carrier signal, QAM allows for the efficient encoding of data, facilitating high data rates and improved spectral efficiency in comparison with alternative modulation schemes, such as frequency shift keying (FSK) and amplitude shift keying (ASK). A single-wire PLC system has been demonstrated between the frequency range of 130 MHz to 20 GHz in [23] for the purpose of smart grid communication, demonstrating the possibilities of much higher carrier frequencies for PLC than is specified within the established HomePlug and IEEE 1901 standards. This paper explores PLC over a range of frequencies for optimal conducted performance, since it is expected to operate in a closed environment where use of licenced bands does not present an issue. The radiated emissions measurements included, provide both the conducted performance and some indication of the level of shielding and battery pack output filtering that would be required if operating in a licenced band.

1.1. Smart cell PLC literature review

The integration of a communication system and sensors within a Li-ion cell is typically referred to as a smart cell. Research is currently ongoing in designing and implementing a smart cell with a appropriate communication system.

A smart cell system using four instrumented 21700-model Li-ion cells in a configuration of two cells in series and two cells in parallel (2S2P) was presented in [28]. Also, in that work, each cell utilised a Texas Instruments THVD8000 PLC modem and microcontroller to measure internal cell temperature and to communicate such data with a master PLC modem at a carrier frequency of 5 MHz. The same PLC modem was also used in [34], where a smart battery monitoring system consisting of four instrumented 21700-model Li-ion cells was demonstrated. It was shown that the PLC network used less power than a similarly configured controller area network (CAN) bus.

In [31], two different commercial RF transceivers were utilised to investigate the performance of PLC communication at 868 MHz and 2.4 GHz in a battery of 8 Li-ion cells. It has been determined that a stable data rate of 150 kbit/s and 250 kbit/s can be achieved with this system, and that wireless communication can be used as a possible fallback where a failure in wired communication occurs due to a cut in the PLC communication bus.

In [32], a Yamar SIG60 commercial PLC modem and a microcontroller was integrated within a Li-ion pouch cell during manufacture in order to create a fully embedded smart cell capable of PLC. Electroimpedance spectroscopy and repeated cell cycling were used to determine that the integration of the embedded system within the cell during manufacture had negligible effect on the performance of the cell. A PLC network of eight instrumented 21700-model Li-ion cells has been shown in [36], whereby a Yamar SIG60 PLC modem was connected to a group of four cells using a separate wired serial universal asynchronous receiver/transmitter (UART) connection. This work is beneficial for communicating data between a small battery to an external data logging system. However, as already stated, for a large-scale battery system, the requirement of separate wired connections on each cell increases complexity and weight.

In [37], a small-scale Li-ion battery system of 18650-model cells was used to demonstrate PLC communication between a single networked cell within a battery and an external BMS. In another work, a PLC system within a Li-ion battery of 28 cells was demonstrated using a receiver and transmitter on either end of the battery [38]. In [39], the characterisation of an 18650-model Li-ion cell as a communication channel for PLC at 100 kHz to 300 MHz was performed using a vector network analyser (VNA) for measuring S21 scattering parameters (i.e., the ratio of a wave transmitted from port 1 and received at port 2, as will be explained later) used to determine the cell impedance and insertion loss. The Li-ion cell was attached to a customised printed circuit board in a shunt-through configuration to improve the connection reliability between the VNA and the cell terminals. It has also been shown that the cell impedance changed with the carrier frequency, and that the cell impedance had reached 40 Ω at 300 MHz.

In another work, an analysis of three different coupling techniques with four Li-ion cells was performed using a VNA and a spectrum analyser to determine the system impedance and received signal strength of the system [40]. Simulation of the use of QAM with PLC for carrier frequencies of 100 kHz to 200 MHz through Li-ion cells under a typical BEV drive load profile has been performed in [33]. In this work, it was shown that existing electrochemical impedance spectroscopy (EIS) of Li-ion cells could be utilised within a simulation to obtain the required data to determine the expected communication performance of in-situ battery PLC. A performance evaluation of PLC with changes in the carrier frequency and the Li-ion cell SoC has been demonstrated in [29]. Both the S21 magnitude of the Li-ion cell communication channel and the error rate of QAM symbols transmitted on this channel were measured at various SoCs to determine the relationship between the S21 magnitude and the PLC performance when the Li-ion changes SoC. This research has demonstrated that the S21 magnitude of the Li-ion cell was proportional to the communication performance of PLC through the Li-ion cell, and that the expected performance of the communication system could be derived from S21 magnitude measurements. In [41], the communication performance of PLC with QAM through Li-ion cells arranged in single cell, two cells in series, two cells in parallel, and two cells in series and parallel, were tested for carrier frequencies of 10 MHz to 200 MHz. Recommendations on the PLC carrier frequency were made for where there were few data errors in PLC communication. However, further work is required to understand the impact of the battery holder and the DC offset circuit used in the methodology presented.

All of the stated established literature perform S21 magnitude and PLC tested on passive Li-ion cells rather than instrumented or smart cells. This fact exists as research is ongoing in safely instrumenting cells during and after manufacture without any safety detriment to the cells. Furthermore, it has been shown that cell instrumentation has negligible effects on the impedance of the cell [12]. In addition, research is currently ongoing in developing a computer system that can be embedded within a Li-ion cell that can transmit embedded sensor data along the bus bar. Therefore, this paper will continue this research direction by using passive Li-ion cells.

A summary of the most important established works on in-situ Li-ion battery PLC is presented in Table 2.

Table 2
Summary of existing works on in-situ Li-ion battery PLC systems.
SIG60 [24] is manufactured by Yamar Electronics Ltd (Yamar, Israel); THVD8000 [25], CC1200 [26], and CC2520 [27] are manufactured by Texas Instruments Inc. (TI, USA).

Experimental summary	Battery configurations	Communication parameters	Reference
Integration of a commercial PLC modem and temperature sensor within a Li-ion cell for a smart cell network.	2S2P	5 MHz, OOK, TI THVD8000	Vincent et al. [28]
Channel and performance analysis of PLC and QAM with changing SoC of a Li-ion battery.	Single Cell	10 - 6000 MHz, QAM	Koshkouei et al. [29,30]
Use of existing commercial RF transceivers for high frequency PLC within batteries using capacitive coupling.	4S, 4P	868 MHz, TI CC1200 and 2.4 GHz, TI CC2520	Marsic et al. [31]
Implementation of an in-situ Li-ion PLC system for the purpose of integration within the cell during manufacture using a commercial PLC modem.	Single Cell	6.5 MHz, Yamar SIG60	Fleming et al. [32]
Performance analysis simulation of an in-situ battery PLC with QAM under a BEV driving load profile.	2S, 2P	0.1 - 200 MHz, QAM	Koshkouei et al. [33]
Use of PLC in a system of four Li-ion cells to communicate cell sensor data to an external data logging system and verified using additional CAN and USB communication using a commercial PLC modem.	2S2P	5 MHz, OOK, TI THVD8000	Vincent et al. [34]
Li-ion battery channel characterisation for an in-situ battery PLC system.	Single Cell	0.1 - 1000 MHz	Talei et al. [35]
Communication of cell instrumentation data to an external data logging system using a commercial PLC modem and wired serial connection to each cell.	4S2P	6.5 MHz, Yamar SIG60	Vincent and Marco [36]
Demonstration of communication between two PLC modems within a small-scale Li-ion battery pack.	6S	1-30 MHz, OOK	Landinger et al. [37]
Li-ion battery modelling and PLC channel characterisation up to 30 MHz for simulation, verified using a real implementation using two PLC modems.	28 Cells	10 MHz, FSK	Talie et al. [38]
Performance of PLC and QAM with varying battery configurations using a VST and VNA for in-situ battery communication performance and channel analysis, respectively.	Single Cell, 2S, 2P, 2S2P	10 - 6000 MHz, QAM	This work.

1.2. Paper contributions

State-of-the-art research has not yet identified changes in PLC performance and channel impedance within a variety of battery configurations (the number of cells in series and/or parallel). Such research is critical in determining the best parameters for a PLC system for smart batteries. Since each BEV manufacturer typically uses a different battery configuration, it is important to understand how changes in channel impedance with battery configuration may cause changes in PLC performance. By understanding the changes in communication performance in various battery configurations, the communication system can be adapted to use the most appropriate parameters of carrier frequency, modulation order, and also to determine whether the use of a repeater within the battery system is required. Furthermore, the characterisation of various battery configurations can be used in conjunction with reconfigurable battery technology [42] to maintain the optimum PLC performance during sudden battery reconfiguration and to disable certain configurations that restrict PLC performance. This PLC system can be used in conjunction with instrumented cells to create a smart cell system that is able to function independent of an external data acquisition system, without an additional wire harness, and can communicate with other smart cells and the BMS to perform safety and performance critical tasks. These tasks include online battery reconfiguration, improved analysis of cell degradation, and active thermal regulation. As already stated, these techniques can improve battery safety by accurately measuring the internal Li-ion cell core temperature and regulate charging and discharge currents using an onboard computer system, or with an external BMS.

In this paper, characterisations of Li-ion cells in four different configurations are carried out and tests on the performance of PLC with carrier frequencies up to 6 GHz are performed to analyse the impact on communication performance with each battery configuration and to determine recommendations on the implementation of next generation connected smart batteries. Furthermore, the effectiveness of QAM is tested as a modern modulation scheme for increased data rate. Such analysis has not been conducted in the established literature. In addition, a configurable cell holder is designed and calibrated to reduce the effects of noise and is utilised within this research to facilitate the characterisation of Li-ion cells. The Li-ion cell configurations selected represent the simplest building blocks that make up a full BEV battery system. By using the methodology and conclusions within this paper, the performance of a prospective PLC system within an actual battery system can be derived. Performing this research on small battery configurations as opposed to large-scale battery systems is advantageous for the following reasons:

- Existing battery systems have not been designed for use with in-situ PLC. As such, the design of the batteries, such as the connections between the cells and to the bus bar, have not been characterised in the context of wired and high frequency communication. Hence, it is practically impossible to accurately determine whether changes in in-situ PLC performance and battery impedance are due to the Li-ion cells, the configuration of Li-ion cells, or due to the connections of the cells and the battery bus bar. In this research, a bespoke configurable cell holder is designed to reduce the effects of the connections between the cells within the battery configuration and to the measurement devices in order to focus on how the configuration of cells and the cells themselves affects the impedance of the communication channel and the performance of the PLC system. This bespoke cell holder uses features such as high frequency SMA connectors and careful PCB routing to reduce the effects of the cell holder on the measurements. In contrast, existing battery systems do not have such features that benefit high frequency communication.
- The small battery configurations characterised in this research can be used to derive the characteristics of large-scale battery systems and future smart battery systems. Performing such characterisation on a specific large-scale battery does not yield the

same benefits, as it would not be clear how further changes to the battery configuration cause changes to the characteristics that affect the in-situ PLC system.

- This research performs measurements of four distinct battery configurations that are within the ±10 V rating of the measurement equipment for battery impedance and communication quality, and the results of this research can be used to determine the expected PLC performance of a large-scale battery and to make requirements on communication parameters and the most suitable battery configuration.

Overall, this method enables an evaluation of the limitations within the communication system, and recommendations are made on the parameters of such a PLC system as well as on the design of a large-scale battery pack. This research benefits the BEV and the smart grid as it allows for smarter energy management using direct PLC between the smart cells within the BEV battery pack directly to the smart grid. This technique in turn grants remote online diagnostics of specific cells, improved safety and performance of the smart battery, and optimal utilisation of the BEV when attached to the smart grid.

The key contributions of this work are as follows:

1. Carrier frequencies of 10 MHz to 6 GHz are investigated in scattering parameter (S-parameter) measurements and real PLC testing with QAM up to orders of 1024, to evaluate their effectiveness of noise rejection and data rate with battery configurations of single cell, two cells in series (2S), two cells in parallel (2P) and a four cell configuration of two cells in parallel and in series (2S2P).
2. A configurable cell holder for 18650-model Li-ion cells is designed to allow for ease of reconfiguration without the removal of the cell from the circuit or requiring re-calibration between measurements.
3. An analysis is provided on the relationships between PLC performance, S-parameter magnitude, and battery configuration, and how the expected data rate may be determined based on these relationships.
4. Recommendations on parameters are made for prospective in-situ PLC systems based upon empirical evidence, such as appropriate carrier frequencies and QAM orders.

2. Experimental details

The Rohde & Schwarz (R&S) ZNA43 vector network analyser (VNA) is used to perform S-parameter measurements of the Li-ion battery configuration as a PLC channel, which enables determining impedance and insertion loss. In this study, the S21 magnitudes are presented to demonstrate the changes in PLC channel performance with carrier frequency and battery configuration. The S21 magnitude is the ratio of the wave transmitted by the VNA at port 1 to the measured wave at port 2. These measurements can be used to determine various Li-ion cell characteristics, such as its impedance and insertion loss. Let the characteristic impedance Z_0 of the VNA be 50 Ω, then the impedance of the cell, Z_{cell}, is calculated by [39]

$$Z_{\text{cell}} = \frac{Z_0 S_{21}}{2(1 - S_{21})} \tag{1}$$

The Insertion Loss, IL, is given by

$$\text{IL} = 20 \log_{10} |S_{21}| \tag{2}$$

Hence, the changes in S21 magnitude of the cell affect the performance of PLC communication. Further details of scattering parameters can be found in the established literature including [43]. The VNA is configured to perform S21 measurements for frequencies of 10 MHz to 6 GHz with a step of 100 kHz, and is 'One-Path Two-Port' calibrated using a R&S ZN-Z129 calibration kit with a single cell holder for the same frequencies to simplify the comparison between the cell configurations.

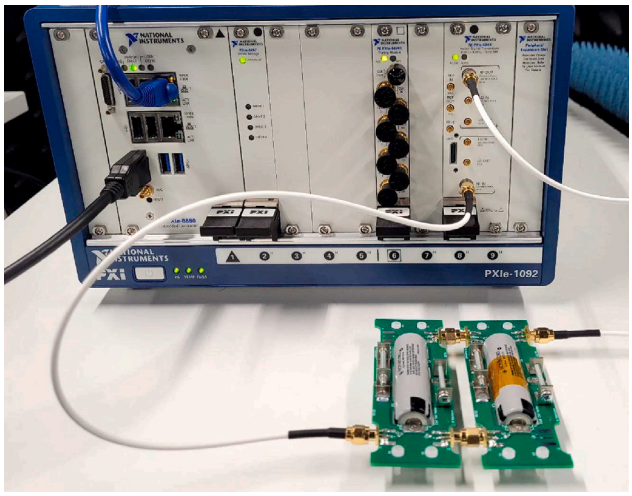

Fig. 1. Cell holders connected in 2P shunt-through configuration to the VST.

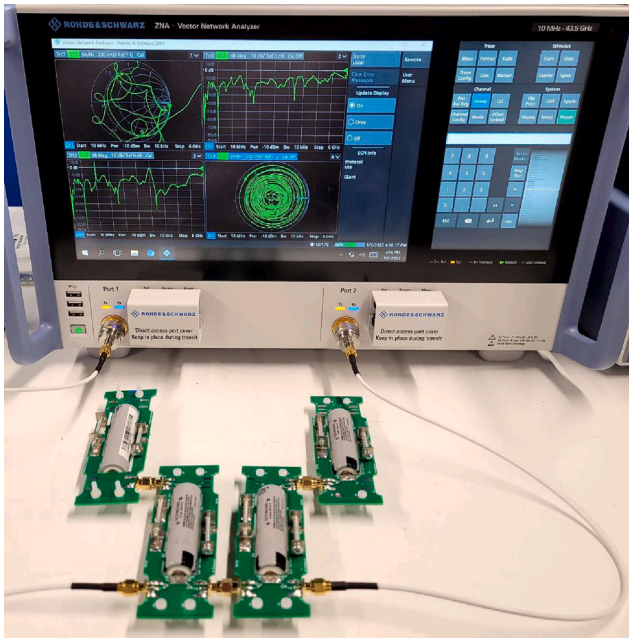

Fig. 2. Cell holders connected in 2S2P shunt-through configuration to the VNA.

These measurements are carried out 20 times for each configuration and are then averaged to reduce the effects of outliers, noise, and interference.

The NI PXIe-5840 vector signal transceiver (VST) is used to perform real PLC testing of the battery with QAM orders of 4, 16, 32, 64, 128, 256, 512, and 1024-QAM. The VST module is installed within an NI PXIe-1092 chassis and operated using an NI PXIe-8880 controller. As described in [29], the VST is configured to transmit 100,000 QAM symbols with a symbol rate of 100 kHz at carrier frequencies of 10 MHz to 6 GHz with a step of 50 MHz. These QAM symbols include pilot symbols required for the VST to perform the synchronisation used by QAM demodulation. Following these pilot symbols are known random data modulated as QAM symbols. The step size used with the VST is higher than that configured with the VNA due to experimental time considerations. The modulated signal is transmitted across the battery with an output power of −27 dBm. The output power of −27 dBm is selected as it has been previously shown in [29] to be sufficiently low to indicate changes in communication performance caused by

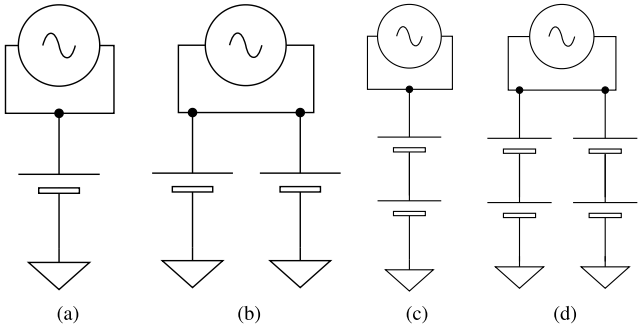

Fig. 3. Circuit diagrams of shunt-through cell holder connections for each Li-ion cell configuration of: (a) Single Cell; (b) 2P; (c) 2S; and, (d) 2S2P.

changes in the cell S21 magnitude. The signal received on the VST input is demodulated into QAM symbols and also further decoded into bits of data. The QAM symbols are compared with a reference QAM constellation to obtain the RMS error vector magnitude (EVM) using

$$\text{RMS EVM}(dB) = 10\log_{10}\left(\frac{\frac{1}{N}\sum_{k=1}^{N}\sqrt{(I_k-\tilde{I}_k)^2+(Q_k-\tilde{Q}_k)^2}}{m_{\text{avg}}}\right) \quad (3)$$

where k is the symbol index, N is the number of symbols, I_k is the in-phase measurement of the kth symbol, Q_k is the quadrature measurement of the kth symbol, and m_{avg} is the average constellation magnitude. Note that $\tilde{I}_k$ and $\tilde{Q}_k$ represent the measured symbols, whereas I_k and Q_k represent the reference symbols. The RMS EVM increases as the magnitude of imperfections between the received QAM symbols and the reference QAM constellation increases. These imperfections may be due to phase distortion and attenuation caused by the communication channel. A high magnitude of RMS EVM generally correlates with increases in corrupted data as the received symbols are decoded incorrectly.

To measure the magnitude of corrupted data, these decoded bits of data received are compared with the transmitted data to obtain the bit error ratio (BER) and the symbol error ratio (SER), which are ratiometric comparisons of the corrupted bits and symbols within the data stream, respectively. Since 100,000 QAM symbols are transmitted in this experiment, the theoretical minimum achievable SER is 10^{-5}.

Each Li-ion cell is clamped within a bespoke shunt-through configurable cell holder as shown in Figs. 1 and 2. This cell holder has been designed to simplify its connection with other cell holders, making cell reconfiguration easier. The design of the cell holder minimises the effect of electromagnetic interference (EMI) on the signal, which includes using short traces and via stitching on the ground plane. This design utilises findings based on simulations and measurements as presented in [44].

Wired communication of high carrier frequencies has been demonstrated in [45], where in carrier frequencies of up to 12 GHz were tested. In this work, it was shown that up to 5 GHz can be transmitted through standard twisted pair copper wire without any radiation effect. Furthermore, this upper limit could be increased by decreasing the twist lengths of the cable.

The shunt-through configuration is used because of its increased accuracy in measuring low-ohmic impedances [35]. In the employed shunt-through configuration, the negative terminal of the Li-ion cell is connected to ground. It is therefore expected that a decrease in the internal resistance of the Li-ion cell will increase the attenuation of the signal. Both the VNA and the VST are connected to the battery in shunt-through configuration at a defined torque via SMA coaxial cables and PCB connectors rated for frequencies up to 12.4 GHz. Fig. 3 shows circuit representations of the shunt-through configurations used in this experiment.

To further reduce the effects of EMI, this experiment is conducted in an anechoic chamber. All of the Li-ion cells used in this research are 18650-type Panasonic NCR18650BD-model [46], and have the same SoC and SoH. The cells are charged at the manufacturers standard charge-rate guideline of 0.3 C to 95 % SoC and left to rest for at least 4 h prior to commencing this experiment to ensure that the core of the cell returns to room temperature after charging. Since the impedance of the Li-ion cell is affected by the SoC, SoH, and temperature, these values are kept constant in this experiment [47]. Due to manufacturing inaccuracies, each Li-ion cell will have slightly varying impedance characteristics, even within the same batch and model. Furthermore, where the VNA is calibrated with a single cell holder, further additional cell holders to form larger battery configurations will cause additional changes in S21 magnitude and phase delay. In this experiment, both the effects of the cells and their configurations on the PLC channel as well as the effects caused by the battery bus bar are of interest. It is important to consider that each battery pack model manufacturer may have different designs, including the shape and size of the bus bar, the type and quality of the cell connections to the power bus, and the cell model used. Hence, in this work, a single calibration is used for all four investigated battery configurations, not correcting for additional scattering from interconnections between individual cell holders. As already stated, using a single calibration profile provides a straightforward comparison between the battery configurations tested.

A smart battery network is expected to communicate cell status (including SoC, SoH, and temperature measurements of the cell core) and instructions to other smart cells and to the external BMS. Since large-scale batteries utilise many thousands of cells, a communication network capable of handling a large amount of data is required to ensure that communication performance does not deteriorate, and that safety and performance events can be communicated with little delay. Hence, a large bandwidth is advantageous in this use case. As such, determining the performance of a PLC system within a battery at high frequencies up to 6 GHz is important in order to select a wide bandwidth that is not susceptible to interference caused by the battery configuration.

As the wavelengths associated to such frequency range start to approach the dimensions from the Li-ion cell and holder, in a first step it is verified to what extent RF power is radiated by them. For this test inside an anechoic chamber, an Electro-Metrics EM-6116 omnidirectional antenna is placed 50 cm away from and oriented in parallel to a Li-ion cell that is clamped within the cell holder and connected to the VST. In addition, RF absorber tiles are placed around the antenna and cell to prevent reflected power from the setup itself affecting the results. The frequency range from 2 GHz to 6 GHz is investigated for radiated emissions, with the EM-6116 having a typical gain of 1.1 dB to 2.3 dB. The cell is placed 50 cm from the antenna to be in its far-field region. The antenna is connected to a R&S FSVA3000 signal and spectrum analyser, which is configured to perform 20 sweeps in a frequency step of 250 MHz, with the maximum power measured to be recorded. The VST is configured to continuously transmit the same stream of 16-QAM symbols used in the main experiment of testing various battery configurations at an output power of −27 dBm, as already described. Table 3 shows the maximum power measured by the spectrum analyser for each frequency tested. In each spectrum only the selected VST carrier frequency can be observed and any possible harmonics or other signals are below the VNA's noise level of approximately −87 dBm.

In addition to this test, the orientation of the cell holder is changed twice such that it is perpendicular, and then upright, to the antenna. For the frequency of 3.25 GHz, which resulted in the highest recorded power radiated in the parallel arrangement, the measured power is −72.84 dBm and −78.24 dBm for perpendicular and upright orientations, respectively.

Taking into account the optimal alignment, the antenna distance, the EM-6116 antenna gain, and assuming a hypothetical transmitting

Table 3
Maximum power radiated by the Li-ion cell and cell holder when it is placed parallel to the antenna. The highest power measured is marked with *. In addition, the calculated free-space path loss and excess loss related to the measurement conditions are presented.

Frequency (GHz)	Received power (dBm)	FSPL (dB)	Excess loss (dB)
2	−80.8	31.1	22.7
2.25	−79.5	32.2	20.4
2.5	−83.6	33.1	23.5
2.75	−83.9	34.0	22.9
3	−78.3	34.8	16.5
3.25	−75.0*	34.9	13.1
3.5	−79.9	35.0	17.9
3.75	−77.0	35.7	14.3
4	−76.1	36.4	12.7
4.25	−82.2	36.8	18.4
4.5	−83.4	37.2	19.2
4.75	−90.1	38.0	25.2
5	−83.6	38.7	17.9
5.25	−86.1	38.9	20.1
5.5	−87.0	39.1	20.9
5.75	−87.0	39.7	20.3
6	−85.0	40.2	17.8

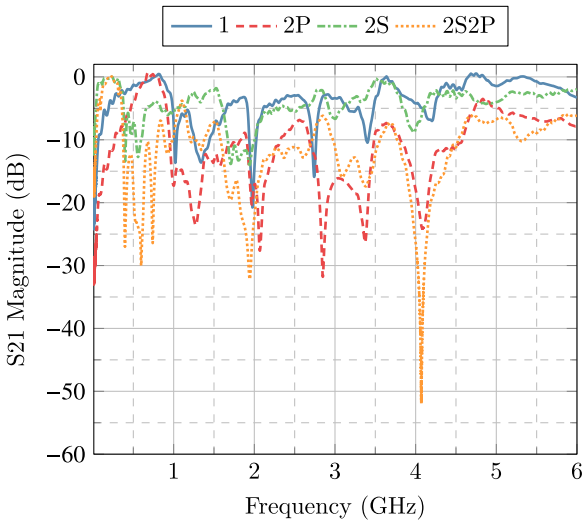

Fig. 4. S21 magnitude of four different battery configurations.

antenna gain of 0 dB for the Li-ion cell, the expected free-space path loss (FSPL) can be calculated using

$$\mathrm{FSPL} = 20\log_{10}(d) + 20\log_{10}(f) + 20\log_{10}\left(\frac{4\pi}{c}\right) - G_{Tx} - G_{Rx} \tag{4}$$

and are provided in Table 3, where d is the distance between the antenna and the Li-ion cell, f is the frequency, c is the speed of light, G_{Tx} is the transmitter (the Li-ion cell) gain and is assumed to be 0, and G_{Rx} is the receiver gain of which the values are obtained from the antenna data sheet. Comparing these values with the differences between the output power of the VST and the received power levels of the VNA for each selected frequency, the excess loss can be determined, which represents the power fraction that is radiated by the Li-ion cell clamped within the cell holder. These tests have thus demonstrated that for all investigated frequencies, the majority of the power is transmitted through the Li-ion cell and not radiated by it.

3. Results and discussion

Using the S21 magnitude and phase shift data of the 20 sweeps performed with the R&S VNA, and by taking into account the standard deviation within such single set of measurements and the reproducibility in clamping the cells within the cell holders, the achieved error margins are ±0.1 dB and ±1.0°, respectively.

3.1. S21 magnitude analysis

The S21 magnitude of the four battery configurations tested are shown in Fig. 4. It can be seen that both the carrier frequency and the battery configuration have a significant impact on the S21 magnitude. However, the battery configurations tested yield similar characteristics, such as peaks in the S21 magnitude at the same frequencies. Further discussion on these similarities is now presented.

As Fig. 4 illustrates, at 10 MHz the S21 magnitudes for all battery configurations begin with varying levels of attenuation of −19 dB, −33 dB, −12 dB and −20 dB for single cell, 2P, 2S and 2S2P battery configurations, respectively. From 10 MHz, a minor trend is observed whereby the single cell and 2P battery configurations show similar properties, as well as 2S and 2S2P. In fact, the S21 magnitudes for both 2S and 2S2P rise close to 0 dB by 200 MHz, indicating that it is an appropriate communication channel as there is little to no loss in signal power using this carrier frequency. On the other hand, the S21 magnitudes for both single cell and 2P rise at a slower rate, and eventually tend close to 0 dB at 650 MHz. At this frequency however, 2S and 2S2P display large reductions in signal power of up to −30 dB, indicating that a change in battery configuration, such as from 1S to 2S for example, will negatively impact the PLC system at 597 MHz. This change in the signal power between battery configuration indicates that this frequency is unsuitable for the smart battery technique of battery reconfiguration unless significant signal conditioning is introduced.

The S21 magnitudes for 2S and 2S2P diverge at 300 MHz, with 2S falling to a minimum of −13 dB at 398 MHz, whereas 2S2P falls much further to a minimum of −27 dB at 396 MHz. Such behaviour may be attributed to differences in multipath fading, whereby an increased destructive interference is seen to occur with the 2S2P configuration in comparison to the 2S configuration at these frequencies. A further two minima occur with both of these battery configurations, whereby 2S shows two small peaks of −9 dB and −13 dB at 474 MHz and 555 MHz, respectively, and 2S2P shows two large peaks of −30 dB and −26 dB at 597 MHz and 739 MHz, respectively. It can also be seen that the 2S2P battery configuration has the most profound influence on the S21 magnitude from 369 MHz to 955 MHz, where the destructive multipath interference, which causes signal attenuation, becomes even more significant. Within this range of carrier frequencies, it is expected that the effect of noise, as in a decrease in signal to noise ratio (SNR), on the communication channel will become more significant. In Section 3.2, which discusses communication error analysis, it will be shown that certain S21 thresholds exist above which the investigated communication channels are capable of successful transmission of a PLC signal with a certain QAM order through these battery configurations tested.

The minor trend of similar properties between 2S and 2S2P, and also with single cell and 2P, which seemingly occurs due to their high and low resistances, respectively, ceases at 955 MHz. Instead, the S21 magnitude for 2S2P and single cell begin to show similarities, whereby another local minimum occurs at 1338 MHz of −12 dB and −14 dB, respectively. It may be concluded that the impact of the addition of cells in the battery configuration on the performance of the communication channel is reduced at this frequency, since the difference in S21 magnitude compared to the single cell is minimal. In addition, at this frequency, a slight peak can also be observed for 2S with an S21 magnitude of −4 dB, which exhibits the least signal attenuation in this comparison. In contrast, 2P displays a similar peak at 1277 MHz, but with the greatest attenuation and an S21 magnitude of −24 dB. This observation aligns with the fact that arranging the cells in series increases the resistance of the signal path to ground and therefore reduces attenuation, whereas the addition of cells in parallel reduces this resistance, hence increasing signal attenuation.

Starting from 1530 MHz, it is observed that the S21 magnitudes of both 2S and 2S2P battery configurations fall from −2 dB and −7 dB to −14 dB and −32 dB at 1943 MHz, respectively. It is also shown that these two battery configurations have a similar trend for the rates at which their S21 magnitudes decrease, and that such trend indicates an increased significance of the destructive interference caused by multipath effects. Furthermore, the S21 magnitudes of the single cell and 2P configuration continue to rise until 1883 MHz, where a much sharper peak then occurs with a minimum S21 magnitude of −21 dB and −20 dB, respectively. After this peak, the S21 magnitudes of all battery configurations rise and eventually settle at 2570 MHz with S21 magnitudes of −3 dB, −7 dB, −5 dB and −12 dB for the single cell, 2P, 2S and 2S2P battery configurations, respectively. This improvement in S21 magnitude suggests that multipath effects still occur, but the timing of the signals at the receiver may be such that a constructive interference is occurring at this carrier frequency. Various factors, such as the length, connections and material of the bus bar may change the magnitude of this effect at various carrier frequencies. Between the frequencies of 2200 MHz to 2700 MHz, the high S21 magnitude indicates a favourable PLC channel with minimal signal loss, suggesting adequate communication quality and reliable data transmission with these battery configurations. This channel allows for a bandwidth of 500 MHz. Despite this fact, it can be clearly seen that the addition of Li-ion cells in parallel reduces the S21 magnitude, thereby indicating that adding further cells to the battery configuration will cause signal attenuation and potentially poor performance and reduced data reliability. It is expected that as the number of cells within the battery configuration increases, the number of signal conditioning utilities, such as signal repeaters, will be added into the communication network. However, the signal output power and/or the number of signal repeaters can be reduced by selecting a bandwidth with a high S21 magnitude as indicated in these battery configuration tests presented here. The performance of this bandwidth is later verified in Section 3.2.

Between 2700 MHz and 2900 MHz, a minimum peak occurs in both single cell and 2P battery configurations, whereas a maximum peak occurs in both 2S and 2S2P battery configurations. These peaks illustrate the minor trends due to multipath fading as already stated, whereby single cell and 2P, and 2S and 2S2P battery configurations demonstrate similar properties.

After the local maximum in 2S and 2S2P battery configurations, a minimum occurs at 3001 MHz and 3091 MHz with S21 magnitudes of −7 dB and −16 dB, respectively. The S21 magnitude for the 2S battery configuration gradually rises after this peak. However, the single cell, 2P and 2S2P battery configurations all have a minimum peak at 3398 MHz, 3373 MHz and 3385 MHz with S21 magnitudes of −10 dB, −26 dB and −17 dB, respectively. This phenomenon shows a deviation in the minor trend of properties between the 2S and 2S2P battery configurations, whereby 2P and 2S2P now have increased their likeliness until 6000 MHz. This suggests that arranging the cells in parallel has a dominant effect on the S21 magnitude compared to arranging the cells in series. At 3640 MHz, a local maximum occurs in all battery configurations, with S21 magnitudes of 0 dB, −7 dB, −1 dB and −8 dB for single cell, 2P, 2S and 2S2P, respectively, again highlighting an appropriate communication channel for all battery configurations. At this frequency, it is expected that the addition of cells in parallel and series will have the least effect on the S21 magnitude, and hence on the PLC performance, in comparison to all the other frequencies tested. However, the addition of cells in parallel clearly has a negative effect on the S21 magnitude in comparison to the addition of cells in series. Therefore, increasing the number of cells in parallel, even at 3640 MHz where the change in S21 magnitude between battery configuration is lowest, may still have a detrimental effect on the PLC system. As it will be stated later, these results can be used to deduce the signal filtering required in order to mitigate the effects of the addition of cells in parallel, which is inevitable in BEV energy storage systems. The S21 magnitudes then decrease, with 2S2P decreasing very sharply and displaying the greatest attenuation for all frequencies tested at 4070 MHz with an S21 magnitude of −52 dB. This low S21 magnitude indicates significant attenuation at this frequency, hence it is most unsuitable for a PLC system as a signal repeater would be required for each additional 2S2P configuration within the battery, thereby increasing complexity, weight and cost of the smart communication system. In addition, at this frequency of 4070 MHz, a large peak also occurs for 2P with an S21 magnitude of −24 dB. After these peaks, the S21 magnitudes all rise above −10 dB and remain nearly frequency-independent, hence increasing their suitability for a PLC system. Between 4450 MHz to 6000 MHz, the S21 magnitude for all battery configurations indicates that due to low signal attenuation on the communication channel, the number of signal repeaters required within the battery system can be reduced, in comparison with other frequencies, such as 4070 MHz, which showed very low S21 magnitude. This range in high S21 magnitude for frequencies of 4450 MHz to 6000 MHz allows for a bandwidth of 1550 MHz. By designing the in-situ battery PLC system to use this bandwidth, either through OFDM or as a wide-band single carrier, the signal conditioning required, such as the use of signal repeaters, can be minimised, which reduces the cost and complexity of integrating a PLC system within a battery.

3.2. Communication error analysis

Since the results of the SER and BER measurements demonstrate identical behaviour, the BER results are omitted for brevity without loss of generality.

Fig. 5 presents the SER of the PLC system with the four battery configurations using an output power of −27 dBm. It is shown that similarly to the S21 magnitude, the SER changes with battery configuration, carrier frequency, and QAM order. As expected, where errors in SER occur, the highest QAM order of 1024-QAM exhibits the highest SER, whereas 4-QAM does not show a single symbol error for all carrier frequencies and battery configurations. Despite this behaviour, there are large carrier frequency ranges where the VST is able to decode all symbols correctly, even for 1024-QAM. Such carrier frequency ranges include 1050 MHz to 2800 MHz, and 4250 MHz to 6000 MHz for the 2P battery configuration. Similarly, the 2S2P battery configuration displays no symbol errors between ranges of 2000 MHz to 3250 MHz, and 4450 MHz to 6000 MHz. In contrast, the single cell and 2S battery configurations show very few occurrences of symbol error, with errors only in 1024-QAM at 10 MHz and 550 MHz for single cell, and in 1024-QAM and 512-QAM at 400 MHz and additionally in 1024-QAM at 2450 MHz for 2S. Crucially, these symbol errors correspond to the instances where the S21 magnitude is most attenuated. For instance, at 400 MHz, the S21 magnitude for the 2S configuration is at a local minimum of −13 dB, which corresponds to the peak in SER with 1024-QAM at the same frequency. Furthermore, both 2P and 2S2P battery configurations demonstrate this trend in high SER with S21 magnitude attenuation. It is also shown that the peaks in S21 magnitude at 395 MHz, 597 MHz and 739 MHz of −27 dB, −30 dB and −26 dB correspond to sharp peaks in SER at 400 MHz, 600 MHz and 750 MHz, respectively. At all three of these peaks an SER of 1 for 1024 and 512-QAM is seen, whereas an SER of 1 for 256, 128, 64, and 32-QAM is only seen for the first two of these peaks. The greatest attenuation in S21 magnitude with 2S2P at 4070 MHz of −52 dB also demonstrates the greatest SER at the same frequency. In fact, the SER of 1024-QAM sharply rises to an SER of 1 at 3950 MHz, and only decreases from 4150 MHz onwards to a minimum SER at 4450 MHz. At 4050 MHz, only 4-QAM does not have an SER of 1, which continues to remain at the lowest SER.

This communication analysis indicates that there is a strong correlation with S21 magnitude attenuation and SER. Moreover, it can be concluded that the addition of cells in parallel significantly reduces the S21 magnitude, which causes signal attenuation and an increase in SER. This increase in SER is most pronounced in higher modulation

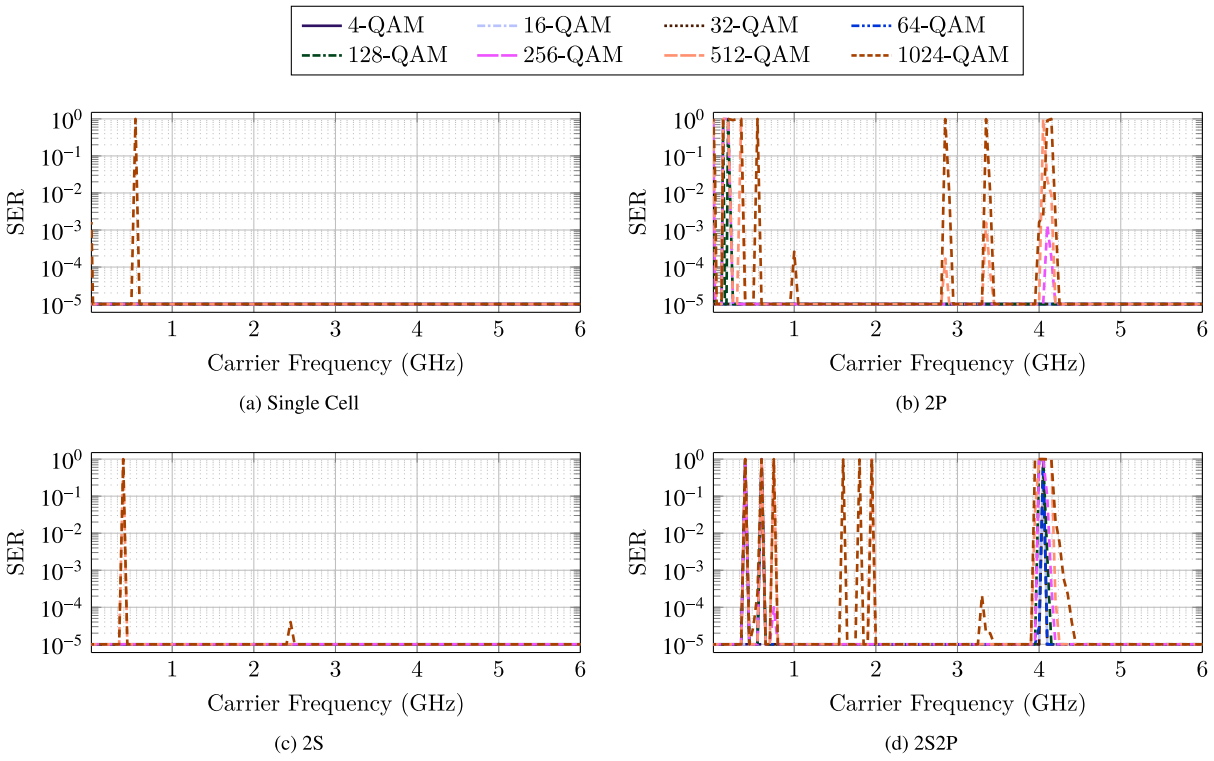

Fig. 5. SER of PLC at −27 dBm through Li-ion cell configurations of: (a) Single Cell; (b) 2P; (c) 2S; and, (d) 2S2P.

orders of QAM, which require a higher signal to noise ratio in order to function correctly without error. Further evidence of these trends are observed in the RMS EVM measurements presented in Fig. 6 whereby rises in RMS EVM correlate with rises in SER. The largest attenuation in S21 magnitude with the 2S2P battery configuration at 4070 MHz corresponds to the high RMS EVM at 4050 MHz of −11 dB for 16-QAM. At the same frequency, the 2P battery configuration reaches a high RMS EVM of −23 dB, whereas 2S and single cell show a low RMS EVM of −42 dB and −44 dB, respectively.

For a VST output power of −27 dBm, the thresholds of S21 magnitude below which symbol errors begin to occur for QAM orders of 16, 32, 64, 128, 256, 512 and 1024 are −30 dB, −27 dB, −26 dB, −25 dB, −24 dB, −21 dB and −16 dB, respectively. At this output power, no symbol error occurred for 4-QAM. This result highlights the trend that with decreasing QAM order, the threshold in S21 magnitude to symbol error continues to increase. Using these relationships between the S21 magnitude, RMS EVM and SER, it is possible to estimate both the SER and RMS EVM based upon measurements of the S21 magnitude of a cell configuration for a given PLC output power, allowing for a much simpler verification procedure during the early design stage of a smart cell system.

3.3. Recommendations

From the stated results it can be deduced that the PLC performance is affected most by the 2P and 2S2P battery configurations, whereas the PLC performance of the 2S battery configuration is least affected in comparison with that of a single cell. This outcome is most likely due to a reduction in the real resistance of the circuit under test, as the two cells in the 2P configuration act as two resistors in parallel. In contrast, placing two cells in series, and hence increasing the real resistance of the circuit, demonstrates slightly improved PLC performance. It is unlikely that the reactance of this circuit has a profound effect on the PLC performance due to the effectiveness of phase compensation processing found in common QAM demodulators, particularly when the magnitude of the received signal is above a certain threshold. In addition to the changing resistance in the shunt configuration of the batteries tested, an impedance mismatch may be causing a multipath effect, whereby the signal propagates onto additional paths causing it to arrive at the receiver at different time intervals as mentioned previously. These effects can cause data corruption and/or loss as measured with SER and RMS EVM in this research. The number of cells in parallel and series must therefore be taken into account when designing a battery pack, as increasing the number of cells in parallel reduces the PLC performance and the achievable data rate, whereas a decrease of cells in parallel will reduce the maximum rated current output of the battery pack. To mitigate this reduction in the PLC performance with the addition of Li-ion cells in the battery configuration, the following techniques can be utilised.

- The addition of cells placed in series should be prioritised over the number of cells in parallel due to the relatively lower impact on the performance of PLC.
- Increasing the output power of the PLC signal to reduce the impact of attenuation caused by the communication channel.
- Adding signal repeaters in the communication system per number of cells. The selection of a frequency and bandwidth that has been demonstrated in this research to show the least attenuation in S21 magnitude, will require fewer signal repeaters than a bandwidth that has high attenuation in S21 magnitude.

Various trends in S21 magnitude between battery configurations are identified which indicate that certain changes in battery configuration do not result in a significant change in S21 magnitude, thereby scarcely affecting the PLC performance in terms of SER either. These trends change in strength with carrier frequency, and in the instance at 3373 MHz, the trend in single cell and 2P battery configuration weakens and changes in favour of the trend in the 2P and 2S2P configurations which remains strong up to 6000 MHz. In fact, at 3600 MHz, the similarity in the S21 magnitude and SER between single cell and 2S, and also for 2P and 2S2P, indicates that the addition of cells in series does not have any significant effect on the PLC channel. Hence,

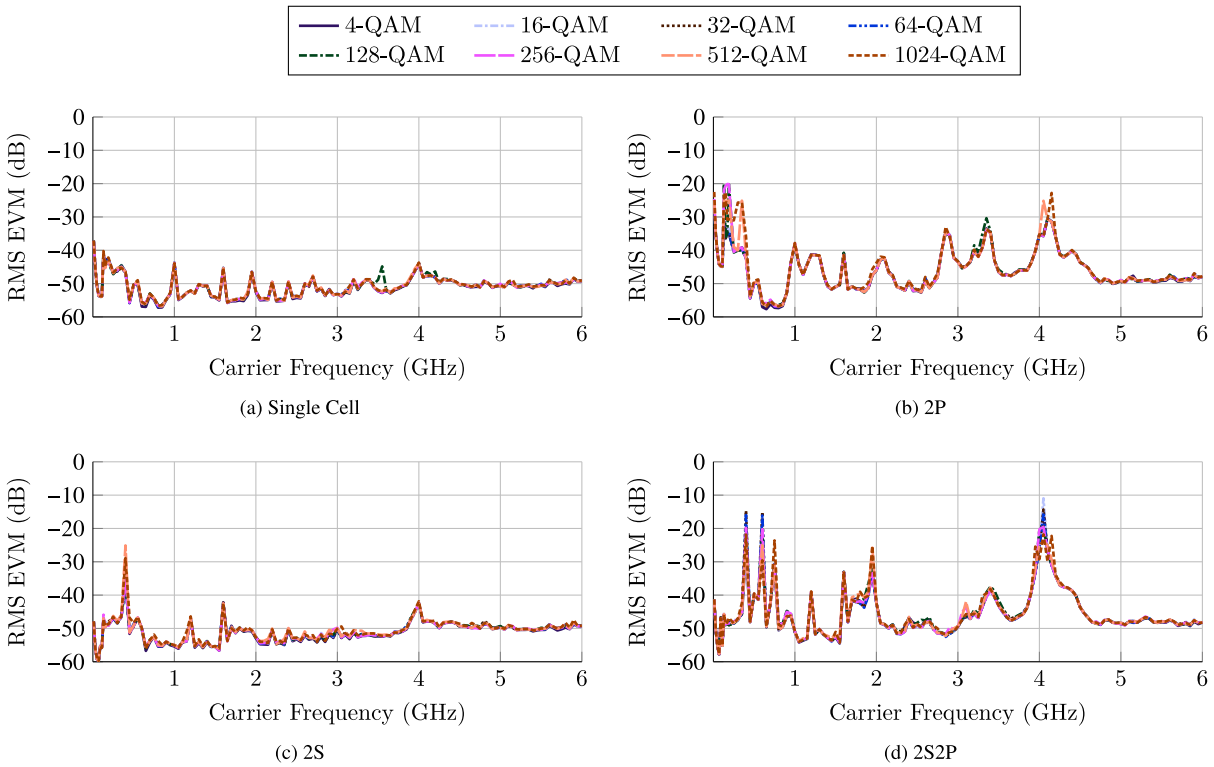

Fig. 6. RMS EVM of PLC at −27 dBm through Li-ion cell configurations of: (a) Single Cell; (b) 2P; (c) 2S; and, (d) 2S2P.

these measurements have highlighted that the addition of cells in series does not impact the expected data rate that can be achieved from PLC within a large-scale battery pack system.

In addition, it can be concluded that suitable carrier frequencies for all investigated battery configurations and QAM orders tested are within the range of 2200 MHz to 2700 MHz, 3500 MHz to 3800 MHz and 4450 MHz to 6000 MHz. Within these ranges, the achievable data rate of the PLC system is expected to be the highest. The range of suitable carrier frequencies may be increased by utilising a lower QAM order, but then the advantages in QAM data rate are also reduced. For large-scale battery systems with an increased number of cells in parallel configuration, signal conditioning techniques may be used to mitigate attenuation, which in turn may increase the cost and complexity of the communication system.

These recommendations are based upon the 18650-model Li-ion cell tested in this research. From existing literature, it can be found that the SoC, SoH, battery model, and battery chemistry have an effect on the cell impedance [48]. It is therefore required that the presented experimentation is performed for each different battery design to consider PLC performance differences caused by these characteristics. These results can be validated by utilising impedance simulations of Li-ion cells to predict the PLC performance [33].

4. Conclusions

In this paper, a PLC network within four battery configurations was evaluated to determine its effectiveness as a smart battery communication system. The 18650-model Li-ion cells were used as a communication channel for in-situ PLC. This technique allows for future smart cells to communicate large amounts of embedded sensor data, such as core cell temperature, to other smart cells in the battery system and to an external BMS, using the existing battery bus bar and without the addition of a wire harness which would increase the complexity, cost, and weight of the battery. The performance of a real large-scale Li-ion battery pack can be derived from the experimental results of the four battery configurations presented in this paper. The use of QAM up to modulation orders of 1024 was analysed for its usability as a modern modulation scheme in this battery system, and is also the highest modulation order defined in the HomePlug AV standard.

This research has demonstrated that battery configuration, carrier frequency, and QAM order, all affect the performance of this PLC system. Based on these results, recommendations for a smart battery PLC network within BEV and smart grid environments have been proposed. Furthermore, the results display trends in the PLC performance with battery configuration, and that certain thresholds in S21 magnitude correspond to the occurrence of symbol errors. For instance, a high S21 magnitude of −16 dB indicates that 1024-QAM PLC is possible at a carrier frequency of 3650 MHz with a bandwidth of ∼300 MHz and as such will exceed the physical layer data rate capabilities found in IEEE 1901, for example [49]. This research thus supports smart cells to communicate vast amounts of sensor data to the BMS and the smart grid using PLC on the bus bar for improved performance, safety, and energy management.

The performance of large-scale battery systems can be determined using the methods used within this experimental work. In addition, an estimation as to the characteristics of large-scale battery systems may be made based upon the four distinct configurations tested within this research. These results demonstrate that whereas some carrier frequencies show significant S21 magnitude attenuation even with two cells in series (2S), other carrier frequencies do not. With these exemplary frequencies, such as 3600 MHz, the EVM and the SER also demonstrated good performance, and therefore a relationship with the measured S21 magnitude. This relationship allows for future designs of smart batteries to be verified for their in-situ battery PLC performance by only requiring a measurement of the communication channel's S21 magnitude. With such measurements, an appropriate carrier frequency can be chosen based on the attenuation recorded in the S21 magnitude, but also allows the selection and magnitude of any signal filtering techniques, such as signal repeaters.

Future work includes a performance analysis of PLC on a Li-ion battery communication bus when the batteries are under various state

of health (SoH) conditions, focusing on how the performance of the PLC network may change as the SoH of the battery degrades with use and time. Furthermore, the differences in PLC between various types of Li-ion cells, such as prismatic and cylindrical, and sizes, such as a 21700-model cell, must yet be evaluated.

CRediT authorship contribution statement

Mahyar J. Koshkouei: Conceptualization, Data curation, Formal analysis, Investigation, Methodology, Project administration, Resources, Software, Validation, Visualization, Writing – original draft, Writing – review & editing. **Erik Kampert:** Conceptualization, Formal analysis, Writing – review & editing. **Andrew D. Moore:** Formal analysis, Writing – review & editing. **Matthew D. Higgins:** Funding acquisition, Writing – review & editing.

Declaration of competing interest

The authors declare the following financial interests/personal relationships which may be considered as potential competing interests: Mahyar J. Koshkouei reports financial support was provided by Engineering and Physical Sciences Research Council

Data availability

Data will be made available on request.

Acknowledgements

This work was supported in part by the UK Engineering and Physical Sciences Research Council (EPSRC) (Grant no. EP/N509796/1 and EP/R513374/1), and in part by the WMG centre High Value Manufacturing Catapult, University of Warwick, Coventry, United Kingdom.

References

[1] Jack N. Barkenbus, Prospects for electric vehicles, Sustainability 12 (14) (2020) 5813, http://dx.doi.org/10.3390/su12145813.

[2] Alvaro Masias, James Marcicki, William A. Paxton, Opportunities and challenges of lithium ion batteries in automotive applications, ACS Energy Lett. 6 (2) (2021) 621–630, http://dx.doi.org/10.1021/acsenergylett.0c02584.

[3] Davide Andrea, Battery Management Systems for Large Lithium Battery Packs, Artech House Publishers, ISBN: 1608071049, 2010.

[4] Manh-Kien Tran, Anosh Mevawalla, Attar Aziz, Satyam Panchal, Yi Xie, Michael Fowler, A review of lithium-ion battery thermal runaway modeling and diagnosis approaches, Processes 10 (6) (2022) 1192, http://dx.doi.org/10.3390/pr10061192.

[5] Foad H. Gandoman, Vahid Nasiriyan, Behnam Mohammadi-Ivatloo, Davood Ahmadian, Electric vehicle integration via smart charging, in: Electric Vehicle Integration Via Smart Charging: Technology, Standards, Implementation, and Applications, Springer International Publishing, ISBN: 978-3-031-05909-4, 2022, pp. 35–48, http://dx.doi.org/10.1007/978-3-031-05909-4_2.

[6] Euan McTurk, Tazdin Amietszajew, Joe Fleming, Rohit Bhagat, Thermo-electrochemical instrumentation of cylindrical Li-ion cells, J. Power Sources (ISSN: 0378-7753) 379 (2018) 309–316, http://dx.doi.org/10.1016/j.jpowsour.2018.01.060.

[7] Ruoqi Zhang, Jiande Wu, Ruichi Wang, Rui Yan, Yue Zhu, Xiangning He, A novel battery management system architecture based on an isolated power/data multiplexing transmission bus, IEEE Trans. Ind. Electron. 66 (8) (2019) 5979–5991, http://dx.doi.org/10.1109/tie.2018.2873143.

[8] Vlad Marsic, Tazdin Amietszajew, Petar Igic, Soroush Faramehr, Joe Fleming, Wireless communication test on 868 MHz and 2.4 GHz from inside the 18650 Li-ion enclosed metal shell, Sensors 22 (5) (2022) 1966, http://dx.doi.org/10.3390/s22051966.

[9] Gaoce Han, Jize Yan, Zhen Guo, David Greenwood, James Marco, Yifei Yu, A review on various optical fibre sensing methods for batteries, Renew. Sustain. Energy Rev. 150 (2021) 111514, http://dx.doi.org/10.1016/j.rser.2021.111514.

[10] Lalit Patnaik, A.V.J.S. Praneeth, Sheldon S. Williamson, A closed-loop constant-temperature constant-voltage charging technique to reduce charge time of lithium-ion batteries, IEEE Trans. Ind. Electron. 66 (2) (2019) 1059–1067, http://dx.doi.org/10.1109/tie.2018.2833038.

[11] Yifei Yu, Timothy Vincent, Jonathan Sansom, David Greenwood, James Marco, Distributed internal thermal monitoring of lithium ion batteries with fibre sensors, J. Energy Storage 50 (2022) 104291, http://dx.doi.org/10.1016/j.est.2022.104291.

[12] B. Gulsoy, T.A. Vincent, J.E.H. Sansom, J. Marco, In-situ temperature monitoring of a lithium-ion battery using an embedded thermocouple for smart battery applications, J. Energy Storage 54 (2022) 105260, http://dx.doi.org/10.1016/j.est.2022.105260.

[13] Joe Fleming, Tazdin Amietszajew, Jerome Charmet, Alexander John Roberts, David Greenwood, Rohit Bhagat, The design and impact of in-situ and operando thermal sensing for smart energy storage, J. Energy Storage 22 (2019) 36–43, http://dx.doi.org/10.1016/j.est.2019.01.026.

[14] Sebastian Steinhorst, Design and verification methodologies for smart battery cells, in: 2016 International Symposium on Integrated Circuits, ISIC, IEEE, 2016, http://dx.doi.org/10.1109/isicir.2016.7829706.

[15] Feng Ji, Li Liao, Tiezhou Wu, Chun Chang, Maonan Wang, Self-reconfiguration batteries with stable voltage during the full cycle without the DC-DC converter, J. Energy Storage 28 (2020) 101213, http://dx.doi.org/10.1016/j.est.2020.101213.

[16] Yunlong Shang, Chong Zhu, Yuhong Fu, Chunting Chris Mi, An integrated heater equalizer for lithium-ion batteries of electric vehicles, IEEE Trans. Ind. Electron. 66 (6) (2019) 4398–4405, http://dx.doi.org/10.1109/tie.2018.2863187.

[17] HomePlug Power Line Alliance, HomePlug 1.0 Technology White Paper, Technical Report, 2005, URL https://www.solwise.co.uk/downloads/files/hp_1.0_technicalwhitepaper_final.pdf.

[18] M.K. Lee, R.E. Newman, H.A. Latchman, S. Katar, L. Yonge, HomePlug 1.0 powerline communication LANs - protocol description and performance results, Int. J. Commun. Syst. 16 (5) (2003) 447–473, http://dx.doi.org/10.1002/dac.601.

[19] Jean Armstrong, OFDM for optical communications, J. Lightwave Technol. 27 (3) (2009) 189–204, http://dx.doi.org/10.1109/jlt.2008.2010061.

[20] Larry Yonge, Jose Abad, Kaywan Afkhamie, Lorenzo Guerrieri, Srinivas Katar, Hidayat Lioe, Pascal Pagani, Raffaele Riva, Daniel M. Schneider, Andreas Schwager, An overview of the HomePlug AV2 technology, J. Electr. Comput. Eng. 2013 (2013) 1–20, http://dx.doi.org/10.1155/2013/892628.

[21] Christina Vlachou, Sébastien Henri, A Practical Guide to Power Line Communications, Cambridge University Press, 2022, http://dx.doi.org/10.1017/9781108890823.

[22] Marcelo S. Alencar, Valdemar C. da Rocha, Communication Systems, Springer International Publishing, 2022, http://dx.doi.org/10.1007/978-3-031-12067-1.

[23] Glenn E. Elmore, Surface wave transmission system over a single conductor having E-fields terminating along the conductor, 2009, US7567154B2.

[24] SIG60: UART/LIN transceiver IC over DC power line, 2022, URL https://yamar.com/product/sig60/.

[25] THVD8000: RS-485 Transceiver with OOK Modulation for Power Line Communication, Texas Instruments Inc., 2021, URL https://www.ti.com/product/THVD8000.

[26] CC1200: Low Power and High Performance Wireless Transceiver, Texas Instruments Inc., 2014, URL https://www.ti.com/product/CC1200.

[27] CC2520: Second Generation 2.4 GHz ZigBee/IEEE 802.15.4 Wireless Transceiver, Texas Instruments Inc., 2007, URL https://www.ti.com/product/CC2520.

[28] Timothy A. Vincent, Begum Gulsoy, Jonathan E.H. Sansom, James Marco, In-situ instrumentation of cells and power line communication data acquisition towards smart cell development, J. Energy Storage 50 (2022) 104218, http://dx.doi.org/10.1016/j.est.2022.104218.

[29] Mahyar J. Koshkouei, Erik Kampert, Andrew D. Moore, Matthew D. Higgins, Impact of lithium-ion battery state of charge on in situ QAM-based power line communication, Sensors (ISSN: 1424-8220) 22 (16) (2022) http://dx.doi.org/10.3390/s22166144.

[30] Mahyar J. Koshkouei, Erik Kampert, Andrew D. Moore, Matthew D. Higgins, Impact of battery state of charge on in-situ power line communication within an intelligent electric vehicle, in: 2022 IEEE 25th International Conference on Intelligent Transportation Systems, ITSC, IEEE, 2022, http://dx.doi.org/10.1109/itsc55140.2022.9921800.

[31] Vlad Marsic, Tazdin Amietszajew, Petar Igic, Soroush Faramehr, Joe Fleming, DC power line communication (PLC) on 868 MHz and 2.4 GHz wired RF transceivers, Sensors 22 (5) (2022) 2043, http://dx.doi.org/10.3390/s22052043.

[32] Joe Fleming, Tazdin Amietszajew, Alexander Roberts, In-situ electronics and communications for intelligent energy storage, HardwareX 11 (2022) e00294, http://dx.doi.org/10.1016/j.ohx.2022.e00294.

[33] Mahyar J. Koshkouei, Erik Kampert, Andrew D. Moore, Matthew D. Higgins, Evaluation of an in situ QAM-based power line communication system for lithium-ion batteries, IET Electr. Syst. Transp. 12 (1) (2021) 15–25, http://dx.doi.org/10.1049/els2.12033.

[34] Timothy A. Vincent, Begum Gulsoy, Jonathan E.H. Sansom, James Marco, A smart cell monitoring system based on power line communication—Optimization of instrumentation and acquisition for smart battery management, IEEE Access 9 (2021) 161773–161793, http://dx.doi.org/10.1109/access.2021.3131382.

[35] Arash Pake Talei, Wolfgang A. Pribyl, Günter Hofer, Considerations for a power line communication system for traction batteries, Elektrotech. Inf.tech. 138 (1) (2021) 3–14, http://dx.doi.org/10.1007/s00502-020-00861-2.

[36] Timothy A. Vincent, James Marco, Development of smart battery cell monitoring system and characterization on a small-module through in-vehicle power line communication, IEEE Access 8 (2020) 220658–220671, http://dx.doi.org/10.1109/access.2020.3043657.

[37] Thomas F. Landinger, Guenter Schwarzberger, Matthias Rose, Stefan Dollhaeubl, Guenter Hofer, Arash Pake Talei, Andreas Jossen, Power line communications in automotive traction batteries: A proof of concept, in: 2020 IEEE International Symposium on Power Line Communications and Its Applications, ISPLC, IEEE, 2020, http://dx.doi.org/10.1109/isplc48789.2020.9115412.

[38] Arash Pake Talie, Wolfgang A. Pribyl, Guenter Hofer, Electric vehicle battery management system using power line communication technique, in: 2018 14th Conference on Ph.D. Research in Microelectronics and Electronics, PRIME, IEEE, 2018, http://dx.doi.org/10.1109/prime.2018.8430304.

[39] Thomas F. Landinger, Guenter Schwarzberger, Andreas Jossen, A novel method for high frequency battery impedance measurements, in: 2019 IEEE International Symposium on Electromagnetic Compatibility, Signal & Power Integrity, EMC+SIPI, IEEE, 2019, http://dx.doi.org/10.1109/isemc.2019.8825315.

[40] Vlad Marsic, Tazdin Amietszajew, Christopher Gardner, Petar Igic, Soroush Faramehr, Joe Fleming, Impact of Li-ion battery on system's overall impedance and received signal strength for power line communication (PLC), Sensors 22 (7) (2022) 2634, http://dx.doi.org/10.3390/s22072634.

[41] Mahyar J. Koshkouei, Erik Kampert, Andrew D. Moore, Matthew D. Higgins, In-situ QAM-based power line communication for large-scale intelligent battery management, in: 2022 7th International Conference on Robotics and Automation Engineering, ICRAE, IEEE, 2022, http://dx.doi.org/10.1109/icrae56463.2022.10056199.

[42] Shaheer Muhammad, M. Usman Rafique, Shuai Li, Zili Shao, Qixin Wang, Xue Liu, Reconfigurable battery systems, ACM Trans. Des. Autom. Electron. Syst. 24 (2) (2019) 1–27, http://dx.doi.org/10.1145/3301301.

[43] Peter J. Pupalaikis, S-Parameters for Signal Integrity, Cambridge University Press, 2020, http://dx.doi.org/10.1017/9781108784863.

[44] Thomas F. Landinger, Guenter Schwarzberger, Andreas Jossen, A physical-based high-frequency model of cylindrical lithium-ion batteries for time domain simulation, IEEE Trans. Electromagn. Compat. 62 (4) (2020) 1524–1533, http://dx.doi.org/10.1109/temc.2020.2996414.

[45] Ergin Dinc, Syed Sheheryar Bukhari, Anas Al Rawi, Eloy de Lera Acedo, Investigating the upper bound of high-frequency electromagnetic waves on unshielded twisted copper pairs, Nature Commun. 13 (1) (2022) http://dx.doi.org/10.1038/s41467-022-29631-8.

[46] Panasonic, The ultimate generation of safe and reliable lithium-ion cell - The new NCR18650BD-Improved, 2021, URL https://mediac.industry.panasonic.eu/p/2021-05/NCR18650BD-Improved_Lithium-ion_Flyer_vers.2.pdf.

[47] Wladislaw Waag, Stefan Käbitz, Dirk Uwe Sauer, Experimental investigation of the lithium-ion battery impedance characteristic at various conditions and aging states and its influence on the application, Appl. Energy 102 (2013) 885–897, http://dx.doi.org/10.1016/j.apenergy.2012.09.030.

[48] Nina Meddings, Marco Heinrich, Frédéric Overney, Jong-Sook Lee, Vanesa Ruiz, Emilio Napolitano, Steffen Seitz, Gareth Hinds, Rinaldo Raccichini, Miran Gaberšček, Juyeon Park, Application of electrochemical impedance spectroscopy to commercial li-ion cells: A review, J. Power Sources 480 (2020) 228742, http://dx.doi.org/10.1016/j.jpowsour.2020.228742.

[49] IEEE, IEEE standard for broadband over power line networks: Medium access control and physical layer specifications, 2020.